Active RIS-aided EH-NOMA Networks: A Deep Reinforcement Learning Approach

Zhaoyuan Shi, Huabing Lu, Xianzhong Xie, Helin Yang, Chongwen Huang, *Member, IEEE*, Jun Cai, *Senior Member, IEEE*, and Zhiguo Ding, *Fellow, IEEE*

arXiv:2304.12184v1 [eess.SP] 11 Apr 2023

Abstract

An active reconfigurable intelligent surface (RIS)-aided multi-user downlink communication system is investigated, where non-orthogonal multiple access (NOMA) is employed to improve spectral efficiency, and the active RIS is powered by energy harvesting (EH). The problem of joint control of the RIS's amplification matrix and phase shift matrix is formulated to maximize the communication success ratio with considering the quality of service (QoS) requirements of users, dynamic communication state, and dynamic available energy of RIS. To tackle this non-convex problem, a cascaded deep learning algorithm namely long short-term memory-deep deterministic policy gradient (LSTM-DDPG) is designed. First, an advanced LSTM based algorithm is developed to predict users' dynamic communication state. Then, based on the prediction results, a DDPG based algorithm is proposed to joint control the amplification matrix and phase shift matrix of the RIS. Finally, simulation results verify the accuracy of the prediction of the proposed LSTM algorithm, and demonstrate that the LSTM-DDPG algorithm has a significant advantage over other benchmark algorithms in terms of communication success ratio performance.

Z. Shi is with the Key Laboratory of Intelligent Perception and Computing of Anhui Province, Anqing Normal University, Anqing, China (e-mail:shizy123@126.com).

H. Lu is with the Key Laboratory of Intelligent Control and Optimization for Industrial Equipment of Ministry of Education, Dalian University of Technology, Dalian 116024, China (e-mail: luhuabing@dlut.edu.cn)

X. Xie is with Chongqing Key Lab of Computer networks and Communication Technology, Chongqing University of Posts and Telecommunications, Chongqing, China(email:xiexzh@cqupt.edu.cn).

H. Yang is with the Department of Information and Communication Engineering, School of Informatics, Xiamen University, Xiamen 361005, China (e-mail: helinyang066@xmu.edu.cn).

C. Huang is with the College of Information Science and Electronic Engineering, Zhejiang University, Hangzhou 310027, China. (e-mail: chongwenhuang@zju.edu.cn)

J. Cai is with the Network Intelligence and Innovation Lab (NI^2L), Department of Electrical and Computer Engineering, Concordia University, Montreal, QC H3G 1M8, Canada (e-mail: jun.cai@concordia.ca).

Z. Ding is with the Department of Electrical Engineering, Princeton University, Princeton, NJ 08544, USA. He is also with the School of Electrical and Electronic Engineering, the University of Manchester, Manchester, UK (e-mail: zhiguo.ding@manchester.ac.uk).

Index Terms —Active reconfigurable intelligent surface, non-orthogonal multiple access, energy harvesting, deep deterministic policy gradient, long short-term memory.

I. INTRODUCTION

With the ability to actively reconfigure the wireless communication environments, the reconfigurable intelligent surfaces (RIS), also named intelligent reflecting surfaces (IRS), has become a focal point in the field of wireless communications [1], [2]. By controlling low-cost passive components, RIS can provide users with an additional set of cascaded channels in addition to the direct link, thus effectively improving communication performance. The RIS is a planar array of a large number of passive elements that are reconfigurable and capable of reflecting electromagnetic signals in the desired manner (controlled by an attached intelligent RIS controller) [3]. Compared with other candidate technologies (such as active relays), RIS has significant advantages in terms of energy consumption, flexible deployment, negligible noise, and economic cost. Therefore, RIS has been widely recognized as a promising paradigm for future 6-th Generation Mobile Communication (6G) networks [4].

The significant capacity gain that RIS brings to wireless communications is mainly derived from negligible noise on the RIS cascade channel [5]. The array gain obtained by an RIS with M elements is proportional to M^2, which is M times more than that achievable by a multiple-input multiple-output (MIMO) system with M antennas at the base station (BS) [6]. However, to obtain such capacity gains, it is usually assumed that the quality of the direct channel (from the transmitter to the receiver) in the system is very poor, or even completely blocked [4], [5], [7]–[9]. Otherwise, the gain of RIS is insignificant or even negligible. The reason behind this phenomenon is the multiplicative fading effect in the cascade channel. Specifically, the path loss of the cascaded channel is the multiplication of the path loss on the BS-RIS link and the RIS-user link, which is usually thousands of times larger than that on the direct channel [10]. Clearly, the multiplicative fading effect reduces the capacity gain brought by RIS arrays and limits the application scenarios of RIS. Therefore, most of the existing RIS-related studies have bypassed this effect and only considered the case where the quality of direct channel is poor or blocked [4], [5], [7]–[9].

In order to overcome fundamental performance bottleneck brought by the multiplicative fading effect in the RIS, a novel concept called active RIS was proposed [6]. The main concept of active RIS is to integrate a power amplifier in each RIS element, thus the RIS can actively amplify

the reflected signal. The introduction of active power amplifiers allows RIS to achieve a sizable increase in capacity, regardless of whether the direct channel is poor or not [11].

Because of the performance advantages, active RIS has attracted a lot of attention in recent years [6], [11]–[14]. Zhang *et al.* developed an active RIS model in [6], which was validated through experimental measurements on a fabricated active RIS element. Based on the model, the authors analyzed the asymptotic performance of active RIS. Finally, a joint transmit beamforming and reflect precoding algorithm was proposed for maximizing sum rate of the active RIS-aided MIMO system. To reduce the energy consumption of active RIS, Liu *et al.* proposed a sub-connected architecture [11], i.e., some RIS elements control their phase shifts independently but sharing the same power amplifier. Furthermore, a beamforming algorithm with the architecture was developed to maximize the energy efficiency of the active RIS-aided system. In [12], the authors fundamentally proved that the multiplicative fading can be transformed into additive fading in active RIS. In [13], You *et al.* defined that in passive RIS, all power amplification factors are the same and $\eta_m = 1, \forall m \in \mathcal{M}$; while in active RIS, each power amplification factor is larger than one due to the introduction of an active amplifier. Besides, the simulation results indicate that active RIS can perform better than passive RIS under optimized placement in most practical scenarios. The work in [14] theoretically compared the active RIS with the passive RIS under the same overall power budget. The theoretical and numerical results showed that the active RIS is superior to passive RIS when the power budget is not very small.

It has been proven that active RIS usually has significant performance advantages over passive RIS. These, however, come at higher energy consumption, which is contrary to the green philosophy of low cost and low energy consumption of RIS. Although [11] proposed a novel energy-efficient structure, it still requires a fixed power supply to provide more energy than the passive RIS. Thanks to the rapid development of green energy technology in recent years [15] and the geographical advantages of RIS installation locations, energy harvesting (EH) technology has naturally become our first choice to address the energy supply problem in active RIS.

In addition, as a promising candidate technology for 6G networks , NOMA technology is effective in improving spectrum efficiency and increasing user connectivity [16]. Therefore, the NOMA technology is introduced in this paper. NOMA allows multiple users of different power levels to communicate simultaneously with the same frequency/time/code resources, and separates the multi-user signals by applying successive interference cancellation (SIC) at the receivers [17]. In [18], Wang *et al.* combines NOMA with EH techniques and applies them

to UAV communication systems. The analytical and simulation results show that the proposed scheme can substantially outperform the alternatives that do not use NOMA and EH techniques.

The combination of NOMA, EH, and RIS can effectively address some challenges of 6G, including spectrum efficiency improvement, energy consumption reduction, and system capacity improvement. Currently, Alanazi has studied RIS-aided EH-NOMA system under Nakagami [19] and Rayleigh fading channels [20]. In both channels, the transmitter harvested radio frequency (RF) energy from another node, which is used to transmit data to multiple NOMA users by using RIS. However, in both papers, each user receives the same phase signal through the RIS. Moreover, the phase and power of RIS were not optimized in these two papers. Diamanti *et al.* studied the problem of maximizing the uplink and downlink rates of Internet of Things (IoT) users in an RIS-aided EH-NOMA system [21], where the IoT users are simultaneous wireless information and power transfer (SWIPT) nodes that receive signals while harvesting energy for their uplink and downlink communications. Zhang *et al.* [22] proposed a RIS-aided cooperative transmission scheme using hybrid SWIPT and transmit antenna selection (TAS) protocols. The simulation work demonstrates the performance advantages brought by the combination of EH, RIS, and NOMA. To optimize the objective, an iterative algorithm was proposed for jointly optimizing the phase of the RIS elements and the power allocation of the IoT users. Unlike the existing literature where the users are the EH node, in this paper the EH technique is employed at the RIS, and the harvested energy is used for the amplification and transmitting of the arriving signals.

In this paper, we focus on the joint control of amplification matrix and the phase shift matrix of the active RIS to maximize the communication success ratio of the RIS-aided EH-NOMA networks, while satisfying the quality of service (QoS) requirement of users, dynamic communication state, and the dynamic energy constraint at the RIS. However, due to the stochastic nature of harvested energy, communication state, and the wireless channel, the traditional optimization algorithms are hardly applicable anymore. Thanks to the rapid development of artificial intelligence, the paradigm of deep reinforcement learning (DRL) offers a promising approach [23], [24]. Due to the powerful learning capability in dynamic unknown environments, DRL has been widely applied to learn the optimal decision policy in wireless communications [25].

In recent years, the DRL algorithms have been studied in the RIS [26]–[31]. Faisal *et al.* investigated an RIS aided full-duplex multiple-input-single-output (MISO) wireless system, where

the beamforming and the RIS phase shift were designed for maximizing the sum rate. A novel DRL algorithm was proposed for optimizing the RIS phase shift [26]. In [27], Liu *et al.* designed a novel double deep Q-network (D3QN) based position-acquisition and phase-control algorithm for the RIS-aided MISO-NOMA network, where an BS periodically observes the environment state for optimizing the deployment and phase shift of the RIS by learning from its mistakes and the feedback of users. In [28], Mu *et al.* investigated the optimization problem of maximizing the effective throughput by optimizing the phase shift of the RIS and the power allocation of the BS in RIS-aided networks by deep learning (DL) and reinforcement learning (RL) algorithms, respectively, where the NOMA and orthogonal multiple access (OMA) schemes were both employed. The simulation results showed that in the RIS-aided network, NOMA achieves a 42% gain compared to OMA, and the RL algorithm also achieves better communication performance than the DL algorithm. In [29], an RIS-aided unmanned aerial vehicle (UAV)-NOMA system was studied, and a DRL algorithm was proposed for the UAV trajectory, RIS configuration, and power control. In [30], a DRL based phase shift optimization algorithm was proposed for RIS aided MISO system, where both half-duplex (HD) and full-duplex (FD) modes were considered. In [31], Wang *et al.* presented a novel and effective DRL-based approach to address joint resource management in a practical multi-carrier NOMA system.

The above DRL based optimization algorithms have achieved good performance in RIS-aided networks. However, these algorithms are based on some perfect assumptions, such as that the agent is accurately informed of the perfect channel state information for all channels [27]–[29] and that users are always in the communication state [26], [28]–[31]. In addition, the states in these DRL algorithms usually contain the phase shift of all RIS elements and (or) all channel gains [26]–[28], [30]. To obtain this information, it is often assumed that a wired link is erected between the RIS controller and the BS, which undoubtedly imposes an additional cost overhead on the RIS-assisted wireless network. Further more, such a DRL state setting always leads to a high complexity of the algorithm, as the number of RIS components in the system is usually large. In addition, to the best of our knowledge, there is no research related to the DRL algorithm for active RIS-aided EH-NOMA networks.

Motivated by the aforementioned background, we design a long short-term memory-deep deterministic policy gradient (LSTM-DDPG) algorithm to control the RIS, which is composed of the LSTM network and the DDPG network. The LSTM network is used to predict the environment features i.e., the user's communication state (UCS), and the DDPG framework

is designed to make controlling decisions based on the prediction result of LSTM. The main contributions of our work are summarized as follows:

- An innovative framework for active RIS-aided EH-NOMA networks is proposed, in which the UCS is dynamically changing and the active RIS is powered by the EH. Besides, the wired connection between the RIS controller and the BS is no longer needed. Based on the framework, we formulate an optimization problem with the objective of maximizing the communication success ratio by jointly controlling the amplification matrix and phase shift matrix of the active RIS.
- A low-complexity LSTM based algorithm is developed for UCS prediction. The prediction is formulated as a time series prediction problem, and the algorithm is trained based on an empirical dataset of long-term observations. After the training, the LSTM network can predict the current communication state information based on the historical UCS.
- A novel DDPG based algorithm is proposed for the joint control of the amplification power matrix and the phase shift matrix of the active RIS. Unlike existing DRL algorithms that require high-dimensional RIS channel and phase shift information, this algorithm takes the prediction results of the LSTM and the currently available energy of the RIS as input states. Besides, as an agent, the RIS controller does not require additional information interaction with the BS or the users throughout the learning process of the algorithm.
- The complexity of the LSTM based UCS prediction algorithm and the DDPG based RIS control algorithm are analyzed. Extensive simulation are provided to verify the high prediction accuracy of the LSTM algorithm, and also demonstrate that the proposed DDPG based RIS control algorithm outperforms the existing benchmarks in terms of the communication success ratio.

The remainder of this paper is structured as follows. The system model is described in Section II. In Section III, LSTM based UCS prediction algorithm is presented. Section IV presents the details of the proposed LSTM-DDPG algorithm. Simulation results and concluding remarks are finally presented in Sections V and VI, respectively.

II. System Model

As illustrated in Fig. 1, an active RIS-aided EH-NOMA communication between a BS and K users is considered. As in [28], [29], the BS and users are all equipped with single antenna, and the locations of the BS, RIS are fixed, which are denoted in a three-dimensional (3D) Cartesian

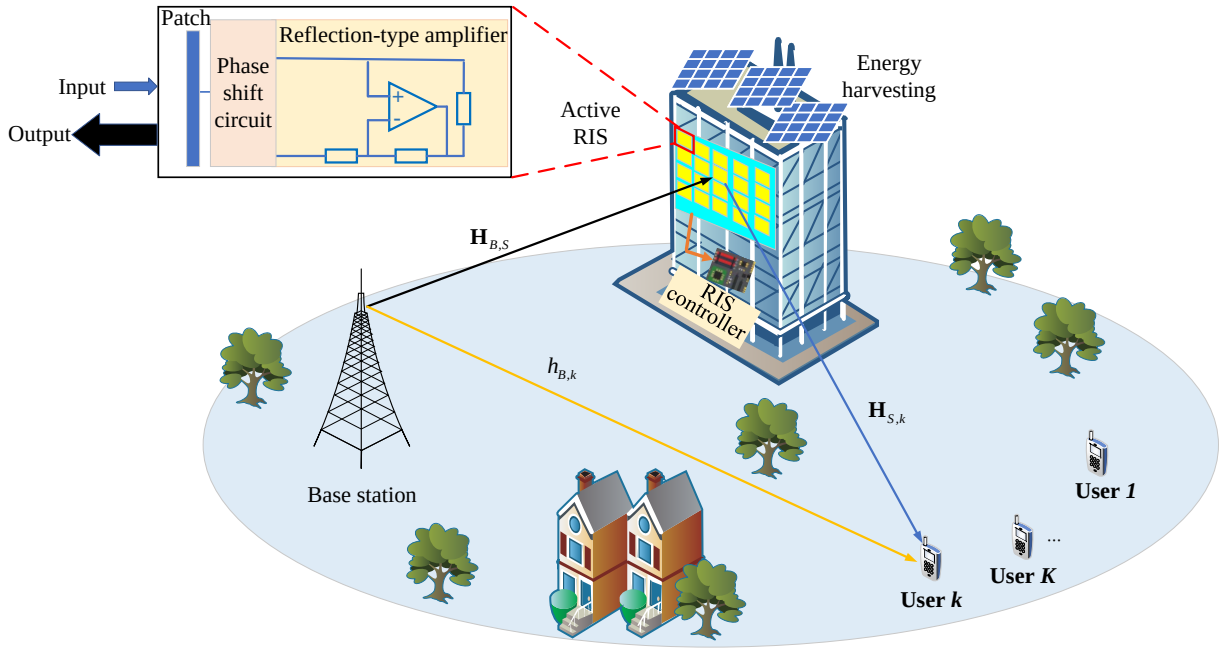

Fig. 1. Illustration of active RIS-aided EH-NOMA networks.

coordinate system. The communication is aided by an active RIS with M active reflecting elements that are installed on the facade of a building [2]. EH is introduced to provide green energy for the active RIS, and NOMA is invoked to further improve the spectrum efficiency of the network [17]. The amplification matrix and phase shift matrix of active RIS are controlled by an attached smart RIS controller.

A. *Active RIS Model*

Similar to existing passive RIS, active RIS can reflect the incident signal by reconfiguring the phase shift. The most essential difference between them is that passive RIS only reflects but does not amplify the incident signal, while active RIS can further amplify the reflected signal [6], [11]. To amplify the signal, an additional amplification device needs to be integrated on the passive RIS as shown in Fig. 1.

Note that there is a clear difference between active RIS and relay-type RIS. In the relay-type RIS, numerous passive RIS elements are connected to an active RF chain and therefore it has some signal processing capability and can transmit the pilot signal independently. However, active RIS is simple in structure and only uses power amplifiers and phase shifting circuits to

control the signal, without signal processing and analysis capability, thus offering significant advantages in terms of delay and cost effectiveness [6], [11].

The key component of an active RIS element is the additionally integrated active reflection-type amplifier, which can be implemented by the existing active components, such as current-inverting converters or some integrated circuits [11]. With reflection-type amplifiers supported by a power supply, the reflected and amplified signal of an M-elements active RIS can be modeled as follows:

$$\mathbf{y}_S(t) = \underbrace{\mathbf{P(t)\Theta(t)x(t)}}_{\text{desired signal}} + \underbrace{\mathbf{P(t)\Theta(t)z}}_{\text{dynamic noise}} + \underbrace{\mathbf{n}_s}_{\text{static noise}}, \tag{1}$$

where $\mathbf{P(t)} = \text{diag}\left(p_1^S(t), p_2^S(t), \cdots, p_M^S(t)\right) \in \mathbb{R}_+^{M\times M}$ is the amplification matrix, wherein each element $p_m^S(t)$ is the amplification factor for the m-th RIS element at slot t (where the superscript S refers to the RIS), and $\mathbf{x} \in \mathbb{C}^M$ is the incident signal. Each element of $\mathbf{P}(t)$ satisfies $0 \le p_m^S \le L$, where L is the maximum amplification factor. The $\boldsymbol{\Theta(t)}$ denotes the phase shift matrix, which can be expressed by

$$\mathbf{\Theta(t)} = \text{diag}(e^{j\theta_1(t)}, e^{j\theta_2(t)}, \cdots, e^{j\theta_M(t)}), \tag{2}$$

where $\theta_m(t) \in [0, 2\pi)$ is the reflection phase shift of the m-th RIS element. Due to the fact that active components are required for signal amplification in active RIS, the thermal noise introduced by active components cannot be ignored. As shown in (1), the noise introduced by the active RIS contains dynamic noise $\mathbf{P(t)\Theta(t)z}$ and static noise $\mathbf{n}_s$, but only $\mathbf{P(t)\Theta(t)z}$ is associated with the amplification matrix $\mathbf{P}$, and $\mathbf{z} \sim \mathcal{CN}(\mathbf{0}_M, \delta_z^2\mathbf{I}_M)$. Therefore, compared with dynamic noise, $\mathbf{n}_s$ can be almost ignored.

Remark 1. *Unlike the definition of the active RIS in [13] with respect to the amplification factor(i.e., $p_m^S > 1$), the value range of p_m^S in this paper is $[0, L]$. This is because the active RIS in this paper is powered by energy harvesting and therefore the harvested energy is dynamic, which makes it difficult to guarantee that the amplification factor of all RIS elements is greater than 1.*

The positions of the BS, RIS, and users are modeled in a three-dimensional (3D) Cartesian coordinate system. Let $\mathbf{H}_{B,S}(t) \in \mathbb{C}^{M\times 1}$ and $h_{B,k}(t) \in \mathbb{C}^{1\times 1}$ denote the BS-RIS and BS-user k channels at t-th time slot, respectively. Correspondingly, $\mathbf{H}_{S,k} \in \mathbb{C}^{1\times M}$ denotes the channel between the RIS to user k. It is assumed that all channels obey a static block fading model in which the channel parameters remain constant within each time slot and vary independently

in the next time slot. Considering that the RIS-assisted communication environment is always scattered and highly correlated, this paper adopts the channel model in [32]. Specifically, the direct link $h_{B,k}(t)$ follows Rayleigh fading distribution. The channels $\mathbf{H}_{S,k}$ and $\mathbf{H}_{B,S}$ are defined as

$$\begin{aligned} \mathbf{H}_{S,k} &\in \mathcal{N}_{\mathbb{C}}(\mathbf{0}, A\mu_{S,k}\mathbf{R}), \\ \mathbf{H}_{B,S} &\in \mathcal{N}_{\mathbb{C}}(\mathbf{0}, A\mu_{B,S}\mathbf{R}), \end{aligned} \tag{3}$$

where A is the area of each RIS element. $\mu_{S,k}$ and $\mu_{B,S}$ are the average large scale path loss of channel $\mathbf{H}_{S,k}$ and channel $\mathbf{H}_{B,S}$, respectively. The path loss is calculated as $C_0(\frac{d}{d_0})^{-\alpha}$ [1], where C_0 denotes the pass loss in the condition of the reference distance $d_0 = 1$ meter (m), $d(d_{B,k}, d_{B,S}, d_{S,k})$ represents the link distance, $\alpha(\alpha_{B,k}, \alpha_{B,S}, \alpha_{S,k})$ denotes the path loss exponent. $\mathbf{R} \in \mathbb{C}^{M\times M}$ represents the normalized spatial correlation matrix which is defined in [32].

B. NOMA Network Model

To improve the spectral efficiency of the system, the NOMA transmission protocol is adopted in this paper, i.e., all users share the same frequency resource. Based on the above channel model, the incident signal of RIS in (1) can be expressed as $\mathbf{x}(t) = \mathbf{H}_{B,S}(t)\sum_{k=1}^{K} p_k U_k(t) x_k(t)$, where p_k is the constant transmit power, x_k is unit power information symbol of user k, U_k is a binary symbol to indicate whether user k is communicating or not. Specifically, $U_k(t) = 1$ indicates that user k is communicating at slot t, otherwise, $U_k(t) = 0$.

As shown in Fig 1, each communicating user k receives the signal from the BS via direct and reflected wireless links. Then, the received signal can be denoted as follows

$$\begin{aligned} y_k(t) =& h_{B,k}\sum_{j=1}^{K} p_j U_j(t) x_j(t) + \mathbf{H}_{S,k}\mathbf{y}_S + n_k \\ =& \left(\underbrace{h_{B,k}}_{\text{direct link}} + \underbrace{\mathbf{H}_{S,k}\mathbf{P}\mathbf{\Theta}\mathbf{H}_{B,S}}_{\text{RIS reflected link}} \right) \sum_{j=1}^{K} U_j(t) p_j x_j(t) + \underbrace{\mathbf{H}_{S,k}\mathbf{P}\mathbf{\Theta}\mathbf{z}}_{\text{noise introduced by active RIS}} + \underbrace{n_k}_{\text{noise introduced at user } k}, \end{aligned} \tag{4}$$

where n_k represents the additive white Gaussian noise (AWGN) at user k with zero mean and variance δ^2. For ease of presentation, the equivalent channel from the BS to the k-th user is defined as $h_k = h_{B,k} + \mathbf{H}_{S,k}\mathbf{P}\mathbf{\Theta}\mathbf{H}_{B,S}$. Therefore, after transmitting through the RIS decorated

integrated channel, the signal received at user k can be calculated as

$$y_k(t) = \underbrace{U_k(t)h_k(t)p_k x_k(t)}_{\text{desire signal}} + \underbrace{\sum_{j\neq k}^{K} U_j(t)h_j(t)p_j x_j(t)}_{\text{inte-user interference}} + \underbrace{\mathbf{H}_{S,k}\mathbf{P}\boldsymbol{\Theta}\mathbf{z} + n_k}_{\text{noise}}. \tag{5}$$

To eliminate the inter-user interference, SIC is carried out. Note that the active RIS cannot perform channel estimation due to the lack of signal processing capability. In this paper, we assume that the system is performing channel estimation for the equivalent channel h_k, rather than estimating $\mathbf{H}_{S,k}$, $\mathbf{H}_{B,S}$ and $h_{B,k}$ separately. Moreover, to be more practical, imperfect SICs due to imperfect CSI is considered in the decoding process of NOMA. Specifically, each user determines decoding order based on the signal strength, which depends on the transmitted power and channel gains of the users. The user with the strongest signal strength will be decoded first. Based on the principle of SIC, each decoded user's signal will be regenerated and then subtracted from the remained signal. The signals of those users who failed to be decoded and also those who have not been decoded will be all regarded as interference [33]. For the decoded user k with a received signal strength of $g_k = U_k(t)|h_k(t)|^2 p_k(t)$, it will be subjected to interference as

$$I_k(t) = \sum_{j\in K, j\neq k} U_j(t)\left[1 - \chi_{jk}(t)d_j(t)\xi\right]|h_j(t)|^2 p_j(t), \tag{6}$$

where χ_{jk} is a binary indicator with $\chi_{jk} = 1$ if the signal strength of the j-th user is stronger than the currently decoded user k, i.e., $|h_j(t)|^2 p_j(t) > |h_k(t)|^2 p_k(t)$, and $\chi_{jk} = 0$ otherwise. Besides, we use $d_j(t) = 1$ to indicate that the j-th user has been successfully decoded, and $d_j(t) = 0$ to indicate that it has failed to be decoded or has not been decoded yet. The parameter $0 < \xi < 1$ is used to characterize the decoding error due to imperfect CSI and hardware limitation. A larger value of ξ indicates a smaller SIC error [34], [35]. Then, the achievable communication rate of user k can be given by

$$R_k(t) = U_k(t)\log_2\left(1 + \frac{g_k(t)}{I_k(t) + \| \mathbf{H}_{S,k}(t)P\boldsymbol{\Theta}(t) \|^2 \delta_z^2 + \delta^2}\right). \tag{7}$$

For successful decoding, it must satisfy the QoS requirements of users as $R_k(t) \geq R_0$, where R_0 is the rate threshold of each user.

C. EH model

Due to the introduction of active components, the active RIS consumes additional power to amplify the reflected signal. In view of the green energy-saving concept of RIS, EH technology

is used to supply energy to active RIS. Considering that RIS is generally installed on the surface of high-rise buildings, where there are geographical advantages for solar and RF energy harvesting. Therefore, this paper adopts a hybrid energy harvesting framework that can overcome the dynamic climate problem in solar energy supply and the problem of collecting too little energy in RF energy supply [36].

For the RF energy, we adopt a non-linear EH model based on the logistic function as in [37]. The total harvested energy is modeled as

$$\begin{aligned} E_{RF}(t) &= \frac{\Psi(t) - E_M\Omega}{1-\Omega}, \quad \Omega = \frac{1}{1+exp(ab)}, \\ \Psi(t) &= \frac{E_M}{1+exp(-a(P_{RF}-b))}, \end{aligned} \tag{8}$$

where E_M is a constant denoting the maximum harvested RF power when the RF EH circuit is saturated. The parameters a and b are constants related to the detailed circuit specifications. $P_{RF} = \|\mathbf{H}_{B,S}\|^2$ denotes the receive RF power.

For the solar energy, we install a fully charged solar panel with an area of S_{sol} on the surface or on top of the building where the RIS is installed. We estimate harvested solar energy by the empirical model presented in [36]. The EH model provides a year-round analysis of solar radiations and relates power levels to a quadratic equation on the time t of the day,

$$E_{sol} = S_{sol}(a1(t+a2)^2 + a3)(1-\sigma_{sol}), \tag{9}$$

where the parameters $a1$, $a2$, and $a3$ are vary seasonally for different months. σ_{sol} is the percentage of cloud cover from weather reports. The harvested RF and solar energy $e^h = E_{RF} + E_{sol}$ will be stored in a rechargeable battery, which is available for signal amplification and reflection at the beginning of next time slot. Let the residual energy stored in the battery at the beginning of time slot t be $E(t)$.

The energy stored in the battery will be scheduled for the amplification and transmission of the incident signal. At time slot t, the energy consumed by the active RIS is

$$e^c(t) = \| \mathbf{P\Theta H}_{B,S} \|^2 + \| \mathbf{P\Theta} \|^2 \delta_z^2. \tag{10}$$

To ensure that the RIS can successfully amplify the incident signal and transmit the amplified signal, it needs to satisfy $0 \leq e^c(t) \leq E(t)$. Then, the $E(t)$ can be evolved as

$$E(t+1) = \min\{E(t) + e^h(t) - e^c(t), E_{max}\}, \tag{11}$$

where E_{max} denotes the maximum capacity of the battery.

D. Optimization Problem Formulation

Due to the stochastic nature of the UCS in the RIS-aided EH-NOMA system and the dynamic nature of the harvested energy at the RIS, a rational control of the RIS is necessary to improve the system performance. Specifically, the amplification matrix $\mathbf{P}$ and the phase shift matrix $\mathbf{\Theta}$ of the active RIS are designed to maximize the successful communication ratio, which is defined as $\frac{\sum_{k=1}^{K} \mathbb{1}(R_k(t) \geq R_0)}{\sum_{k=1}^{K} U_k(t)}$. The $\mathbb{1}(\cdot)$ is the indicator function, when the condition $(\cdot)$ is satisfied, it is equal to 1, otherwise it is 0. Then, the optimization problem can be formulated as follows

$$
\begin{aligned}
\textbf{(P1):} \quad & \max_{\mathbf{P},\mathbf{\Theta}} \frac{\sum_{k=1}^{K} \mathbb{1}(R_k(t) \geq R_0)}{\sum_{k=1}^{K} U_k(t)} \\
& \text{s.t. } U_k(t) \in \{0,1\}; && (C1) \\
& \quad R_k(t) \geq R_0; && (C2) \\
& \quad 0 \leq e^c(t) \leq E(t); && (C3) \\
& \quad E(t+1) = \min\{E(t) + e^h(t) - e^c(t), E_{max}\}; && (C4) \\
& \quad 0 \leq p_m^S \leq L, \quad \theta_m \in [0, 2\pi), && (C5)
\end{aligned}
$$

where $(C2)$ denotes to the QoS requirement for each user. $(C3)$ defines and limits the energy consumed by the RIS which can be supplied by the stored energy. $(C4)$ corresponds to the energy extrapolation principles. $(C5)$ defines the constraints on the amplification factor and phase shift in the active RIS.

III. LSTM BASED PREDICTION ALGORITHM

We propose an LSTM-DDPG algorithm to solve the optimization problem $(\mathbf{P1})$ for RIS controlling. As shown in Fig. 2, the LSTM-DDPG algorithm is composed of the LSTM network and the DDPG framework. The LSTM network is used to extract the active RIS-aided EH-NOMA network features and the DDPG framework is adopted to make controlling decisions.

In this section, we first introduce a dynamic UCS model, which is quite different from the assumption that users are always in a communication state in most of the existing literature. Then an LSTM based algorithm is designed for UCS prediction.

A. Dynamic Communication State

In most existing related works, the users are usually assumed to be in a state of communication all the time, i.e., the users always have data to transmit. Such absolute assumption greatly reduces the dynamics and complexity of the system, thus reducing the difficulty of the associated network research. However, in practical wireless communication systems, such as IoT, vehicular networks, wireless sensor networks, and mobile communication networks, users will not always have data to transmit. Therefore, in this paper, the UCS are assumed to be dynamic. In each time slot, different users communicate based on different probabilities. And the probabilistic data of each user is assumed to be generated based on an independent random walk model [38].

In general, the UCS information can be obtained by analyzing real-time pilot signals in wireless networks. However, due to hardware limitations, the active RIS cannot handle the pilot signal [6], [11]. Therefore, it cannot be informed of the dynamic UCS, nor can it be informed of the channel information of both BS-RIS and RIS-users links through the pilot signals. However, the channel information or the UCS are critical to RIS control [39].

Remark 2. *A large number of RIS elements makes it too difficult to estimate the BS-RIS and RIS-users channels. And considering that the positions of the BS, RIS, and users are fixed, the fluctuation of channel information is smaller than the fluctuation of user communication states. Therefore, to control the active RIS, LSTM is adopted to predict the UCS.*

LSTM is an improved version of recurrent neural networks (RNN). Unlike RNN which can only consider some recent states, by introducing the forget gates and input gates, LSTM is able to remember useful states in the long term and can also choose to forget some insignificant states. Therefore, LSTM is often preferred when dealing with long-term time-dependent problems.

B. LSTM based Prediction Algorithm for UCS

As an enhanced recursive network, LSTM can connect historical information to the current task. In this paper, since the communication probability of a user varies between each time slot, we express it as a time series when predicting the communication probability of each user. The time series data are the input to LSTM along the chain structure in a forward direction. We define the dynamic series of a user as $\mathbf{D} = [\ \mathbf{d}(1),\ \mathbf{d}(2), \cdots,\ \mathbf{d}(T_p)]$, where $\mathbf{d}(t) = [\Pr(t - T_s), \Pr(t - T_s + 1), \cdots, \Pr(t-1)]$ are the time series of the input LSTM, and $Pr_k(t)$ is the communication probability of one user at slot t. T_p is the total number of samples collected, and T_s is the time interval. Note that since the prediction algorithm for the communication state

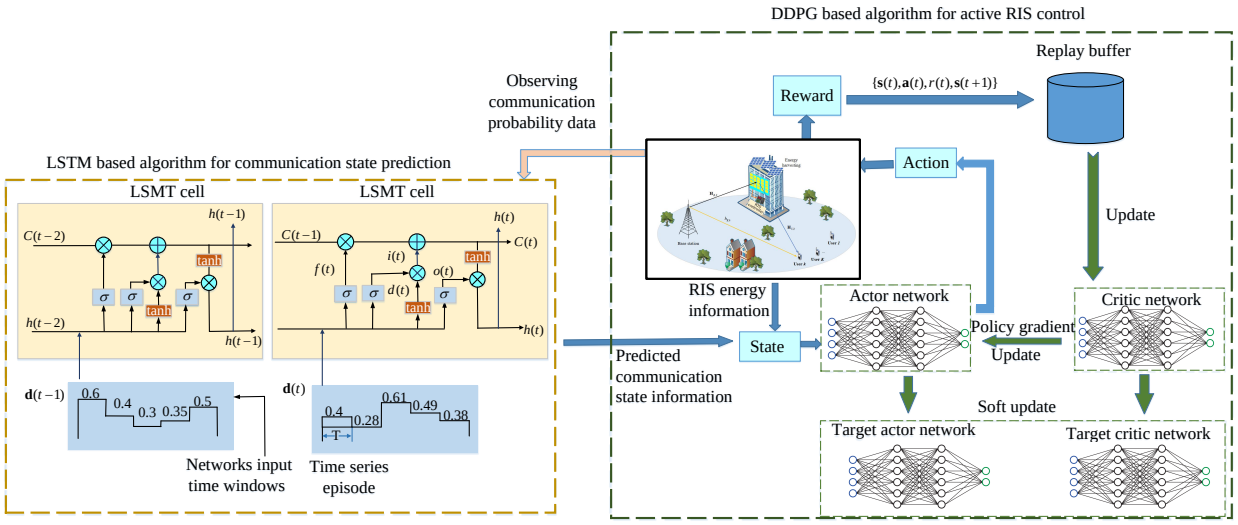

Fig. 2. Structure diagram of RIS control algorithm based on LSTM-DDPG.

is the same for each user, the user identifier k is implicitly removed in this section for ease of presentation.

As shown in Fig. 2, we use the classical LSTM structure [38], [40]. Each LSTM cell contains several hidden layers, which are forget gate, input gate, and output gate.

Forget gate: The first layer is forget layer, which is also known as $f(t)$. The main role of the forget gate is to decide which parts of the cell state $C(t-1)$ of the previous moment will be saved in the current state $C(t)$. It consists of the information passed from previous layer $h(t-1)$ and current input $\mathbf{d}(t)$ with weights $\hat{\mathbf{w}}^f$, $\mathbf{w}^f$, and bias $\mathbf{b}^f$, which can be expressed as

$$f(t) = \sigma\left(\mathbf{w}^f(t)\mathbf{d}(t) + \hat{\mathbf{w}}^f(t)h(t-1) + \mathbf{b}^f(t)\right), \tag{12}$$

where σ represents the gate activation function which is normally sigmoid function. Due to the control of the forget gate, the LSTM can save information from a long time ago.

Input gate: The input gate is used to prevent irrelevant content from entering the memory. It is used to determine how much of the input $\mathbf{d}(t)$ at the current moment will be saved into the state $C(t)$ of the LSTM layer. The input gate is achieved by a 'sigmoid' function and a 'tanh' function, which can be given as follow

$$\begin{aligned} i(t) &= \sigma\left(\mathbf{w}^i\mathbf{d}(t) + \hat{\mathbf{w}}^i(t)h(t-1) + \mathbf{b}^i(t)\right), \\ d(t) &= \tanh\left(\mathbf{w}_k^d\mathbf{d}(t) + \hat{\mathbf{w}}^d(t)h(t-1) + \mathbf{b}^d(t)\right). \end{aligned} \tag{13}$$

Output gate: The output gate is used to control how much of the current state $C(t)$ is fed into the output $X(t)$. From Fig. 3, we can see that $C(t-1)$, as the output state of the previous LSTM layer, will be fed into the current LSTM layer, and the output state $C(t)$ of the current LSTM layer also passes the next LSTM layer. The output state at current time t of the layer can be updated as

$$C(t) = f(t) \otimes C(t-1) + i(t) \otimes d(t). \tag{14}$$

The output is also achieved by the sigmoid function and 'tanh' function, which can be calculated as

$$\begin{aligned} o(t) =& \sigma\left(\mathbf{w}^o(t)\mathbf{d}(t) + \hat{\mathbf{w}}^o(t)h(t-1) + \mathbf{b}^o(t)\right), \\ h(t) =& \, o(t) \otimes \tanh(C(t)). \end{aligned} \tag{15}$$

With the network output $h(t)$, the estimate communication probability can be obtained as

$$\hat{Pr}(t) = \mathbf{w}'(t)o(t) \otimes \tanh(C(t)), \tag{16}$$

where $\mathbf{w}'$ is the regression coefficient. The $\mathbf{w}'$ and the above parameters can be obtained by the real-time recurrent learning algorithm.

Based on the above three types of gate hidden layers, the LSTM can predict the time series of users' communication probabilities based on the real communication information and the previously estimated communication probabilities. By assuming that the estimate output of the LSTM at moment t is $\hat{\Pr}(t)$, and the observed true communication probability at that moment is $\Pr(t)$, then the loss function can be calculated as

$$\text{Loss}(\boldsymbol{\theta}_l) = \frac{1}{T_p}\sum_{t=1}^{T_p}\left(\Pr(t) - \hat{\Pr}(t)\right)^2, \tag{17}$$

where $\boldsymbol{\theta}_l$ denotes network parameters of the LSTM network. Note that it is assumed that the real communication probability data used for training is available through observation, and such an assumption is often used in probabilistic data prediction algorithms [38].

The Algorithm 1 specifies the training and application process of the proposed LSTM based prediction algorithm, which is trained and applied in the RIS controlled. After training convergence, this LSTM based prediction algorithm will be applied to the prediction of UCS. The algorithm remedies the hardware deficiency of the active RIS. Note that in the LSTM-based UCS prediction algorithm, the input to the algorithm is continuously updated historical data. Specifically, the information related to the UCS at the current moment is transformed into the historical data at the next moment [38], [40].

Algorithm 1 The training and application process of the LSTM based prediction algorithm

Training Process:
Input: Training data: 70% of the true communication probability sequence $\mathbf{D}$.
Output: Trained LSTM model, i.e., the optimal network parameters $\boldsymbol{\theta}_l^*$.
Initialization: Initialize the networks parameters $\boldsymbol{\theta}_l$.
for each episode **do**
  Choose the network input $s(t)$ from the observed training data;
  Obtain the output of the last LSTM layer $h(t)$, and calculate the estimate output $\hat{\Pr}(t)$;
  Calculate the loss function $\text{Loss}(\boldsymbol{\theta}_l) = \frac{1}{T_p}\sum_{t=1}^{T_p}\left(\Pr(t) - \hat{\Pr}(t)\right)^2$;
  Update network parameters $\boldsymbol{\theta}_l$ by minimizing the loss function.
end for
Application Process:
Input: Probability of communication for the previous 5 time slots.
Output: The predicted communication state of the user at the current moment.
for each step t **do**
  Input the previous 5 time slot communication probability data to the LSTM networks;
  The LSTM output the estimated communication probability $\hat{\Pr}(t)$;
  Obtain the UCS $\hat{U}(t)$ based on the estimated probability.
end for

IV. LSTM-DDPG BASED ALGORITHM FOR ACTIVE RIS CONTROL

In this section, we first model optimization problem as a Markov decision processes (MDPs). Then a DDPG algorithm is designed for controlling the amplification and phase shift matrix.

A. MDPs Formulation

The optimization problem (**P1**) can be formulated as an MDPs, which consists of an agent, a set of environment sate $\mathbf{s}(t)$, a reward function $R(t)$, and a set of action $\mathbf{a}(t)$.

Agent: Considering that the optimization objects of problem (**P1**) are the amplification matrix $\mathbf{P}$ and the phase shift matrix $\boldsymbol{\Theta}$ of RIS, it is natural to choose the RIS controller as the only agent for the system.

Environment state: Due to the simple structure of the active RIS, it does not have the ability to analyze and process the pilot signal. Therefore, the agent is unable to obtain the channel information of BS-RIS and RIS-user links. Stepping back, we use the predicted communication state $\hat{U}_k(t), \forall k \in K$ of all users as part of the environment state.

Besides, since the active RIS is powered by the EH, i.e., the available energy $E(t)$ is dynamic, which has a significant impact on the decision making of the agent. Therefore, the currently

available energy value $E(t)$ at the RIS is designed as part of the state. In summary, the environmental state of the RIS-aided EH-NOMA system at slot t can be expressed as

$$\mathbf{s}(t) = \left[\hat{U}_1(t), \hat{U}_2(t), \cdots, \hat{U}_K(t), E(t)\right]. \tag{18}$$

Clearly, at the beginning of each time slot, the predicted communication state $\hat{U}_k(t), \forall k \in K$, and remaining battery energy $E(t)$ can be locally observed by the agent.

Action: The action is composed of two matrices, the amplification matrix $\mathbf{P}$ and the phase shift matrix $\mathbf{\Theta}$, which is naturally defined as

$$\mathbf{a}(t) = \left[p_1^S, p_2^S, \cdots, p_M^S; \theta_1, \theta_2, \cdots, \theta_M\right]. \tag{19}$$

The element p_m^S in $\mathbf{P}$ and the element θ_m in $\mathbf{\Theta}$ characterize the power amplification and phase of the m-th RIS element, respectively. And they satisfy

$$0 \leq p_m^S \leq L, \quad 0 \leq \theta_m < 2\pi, \quad \forall m \in M. \tag{20}$$

In addition, since the RIS is powered by the EH, its available energy is dynamic and limited. This will lead to the fact that the available energy may not be able to support some of the actions taken by the agent in the early stages of training. Therefore, in the training of the DRL, when the agent makes an action decision at each time slot, the RIS first checks whether its available energy is sufficient to perform the action. If it is not enough, the action needs to be adjusted as follows

$$\left[\bar{p_m^S}(t), \quad \bar{\theta_m}(t)\right] = \begin{cases} \left[p_m^S(t), \quad \theta_m(t)\right] & e^c(t) \leq E(t) \\ \left[\frac{1}{L}p_m^S(t), \quad \theta_m(t)\right] & e_0^c(t) \leq E(t) < e^c(t), \\ [0, \quad 0] & e_0^c(t) > E(t) \end{cases} \tag{21}$$

where $e_0^c(t) = ||\mathbf{\Theta}\mathbf{H}_{B,S}||^2 + ||\mathbf{\Theta}||^2\sigma_z^2$ is the energy consumed by RIS without power amplification (i.e. $0 \leq p_m^S \leq 1$). Obviously, the design and adjustment strategy of the action vector can guarantee the constraints on energy harvesting, power amplification, and phase shift in the optimization problem (**P1**).

Reward function: In the DRL algorithm, the reward function plays a crucial role in motivating agent to find optimal policy faster. Considering that the objective of the optimization problem (**P1)** is to maximize the successful communication ratio, a brief reward function is designed as follows

$$R(t) = r(\sum_{k=1}^{K} \mathbb{1}_{R_k(t) \geqq R_0}), \tag{22}$$

where r is a positive multiplier greater than 1 that gives the agent an appropriately larger reward to speed up the algorithm training. Clearly, to get higher rewards, the agent will try to learn a better policy to achieve a higher successful communication ratio.

B. LSTM-DDPG based RIS Control Algorithm

1) DDPG : For the formulated MDPs framework, as indicated by (18) and (19), the state and action space are both continuous and multi-dimensional. Therefore, compared to value based DRL algorithms, such as Q learning and DQN algorithms [41], the policy gradient DRL algorithms, such as AC and DDPG are more suitable for the optimization problem in this paper. The structures of the DDPG and AC algorithm are similar, both consisting of an actor network and a critic network, except that DDPG has two more target networks, i.e., the target actor network and the critic network. In fact, DDPG is an upgraded algorithm of AC, which combines the advantages of DQN and AC. Therefore, the DDPG algorithm is adopted in this paper for the design of active RIS. As shown in Fig. 3, four DNNs are included in the DDPG algorithm to learn the optimization policy for the active RIS, which are listed as follows:

Actor network: The actor network is also known as the policy network with parameters $\boldsymbol{\theta}_\mu$. It is dedicated to learning the decision parameterized policy μ of the whole algorithm. Based on the learned policy, it outputs the corresponding action $\mathbf{a}(t) = \mu\left(\mathbf{s}(t) \mid \boldsymbol{\theta}_\mu\right)$ for any environmental state $\mathbf{s}(t)$.

Critic network: The critic network is also known as the Q network with parameters $\boldsymbol{\theta}_Q$. The main role of the critic network is to evaluate the policy μ learned by the actor network and thus guide the direction of parameter updates for the actor network. It takes the current environment state $\mathbf{s}(t)$ and action $\mathbf{a}(t)$ as the network input, and outputs the corresponding state-action value $Q(\mathbf{s}(t), \mathbf{a}(t) \mid \boldsymbol{\theta}_Q)$.

Target networks: The target actor network with parameter $\hat{\boldsymbol{\theta}_\mu}$ and the target critic network with parameter $\hat{\boldsymbol{\theta}_Q}$ are introduced to calculate the target action and the target Q value Q', respectively. They can effectively improve the stability and convergence of the DDPG algorithm. The network structures of the target actor (critic) network and the main actor (critic) network are exactly the same. The difference between the two types of networks is that there is a time interval on the update of the network parameters. Specifically, the target network parameters are

updated through soft updating every C steps as follows

$$\begin{aligned}\boldsymbol{\theta}_{\mu'}(t) &= \tau_\mu \boldsymbol{\theta}_\mu(t) + (1-\tau_\mu)\boldsymbol{\theta}_{\mu'}(t),\\ \boldsymbol{\theta}_{Q'}(t) &= \tau_Q \boldsymbol{\theta}_Q(t) + (1-\tau_Q)\boldsymbol{\theta}_{Q'}(t),\end{aligned} \tag{23}$$

where $0 < \tau_\mu \ll 1$ and $0 < \tau_Q \ll 1$ denote the soft updating factors.

2) The training process of LSTM-DDPG based control Algorithm: In each time slot t, the agent observes the active RIS aided EH-NOMA system and obtains an environment state $\mathbf{s}(t)$. The state is then fed into the actor network, which outputs the corresponding action $\mathbf{a}(t)$. In order to fully explore the environment, the output actions need to be noised during the training, i.e.

$$\mathbf{a}(t) = \mu\left(\mathbf{s}(t) \mid \boldsymbol{\theta}_\mu(t)\right) + n_o(t), \tag{24}$$

where $n_o(t)$ is the exploration noise, which can be expresses as

$$n_o(t) = \begin{cases} n_{ini} - t * \varphi, & n_o(t) > n_{end} \\ n_{end}, & \text{otherwise} \end{cases}, \tag{25}$$

where n_{ini}, n_{end}, and φ represent the maximum exploration noise, the minimum exploration noise, and the decreasing factor of the exploration noise, respectively. Note that the action output by the actor network are first noise-added based on (25), and then the action are adjusted based on (21). Then, the agent obtains the corresponding reward $R(t)$, and the system environment moves to the next state $\mathbf{s}(t+1)$. Based on this exploration, the agent can obtain an experience tuple $[\mathbf{s}(t), \bar{\mathbf{a}}(t), R(t), \mathbf{s}(t+1)]$, which will be stored in the experience replay memory $\mathcal{D}$ and used for the training of the neural network. The main idea of training is to obtain an optimal RIS control policy $\mu*$, which can be realized by updating the parameters of actor and critic networks until convergence.

To updating the actor and critic networks, the Ω-size mini-batch will be randomly sampled from $\mathcal{D}$. The update of critic network parameters is achieved by reactive transfer of TD errors, and the loss function is defined as

$$L(\boldsymbol{\theta}_Q) = \frac{1}{\Omega}\sum_{i=1}^{\Omega}\left[Q'(i) - Q\left(\mathbf{s}(i), \mu(\mathbf{s}(i)|\boldsymbol{\theta}_\mu)|\boldsymbol{\theta}_Q(i)\right)\right]^2, \tag{26}$$

where Q' is the target value of the state-value function (i.e., the output of target critic network), which can be calculated by the Bellman equation as

$$Q'(i) = R(i) + \gamma \max_{\mathbf{a}} Q'\left(\mathbf{s}(i+1), \mu'(\mathbf{s}(i+1)|\boldsymbol{\theta}\mu'(i))|\boldsymbol{\theta}_{Q'}(i)\right). \tag{27}$$

Then by minimizing the loss function (26), the critic network parameters can be updated as

Algorithm 2 Training Process of LSTM-DDPG Algorithm

Input: The LSTM networks with network parameters $\boldsymbol{\theta}_l^*$, the learning rate β_μ and β_Q, the soft updating factor τ_μ and τ_Q.
Output: The trained actor and critic networks with optimal network parameters $\boldsymbol{\theta}_\mu^*$ and $\boldsymbol{\theta}_Q^*$.
Initialize : Empty the replay memory $\mathcal{D}$, $\boldsymbol{\theta}_\mu$ and $\boldsymbol{\theta}_Q$ with random weighs and bias.
for each episode $T = 1, \ldots, T^{all}$ **do**
  Reset the RIS-aided EH-NOMA system;
  for each step $N = 1, \ldots, N^{all}$ **do**
    Predict the UCS by the trained LSTM network;
    Observe the state $\mathbf{s}(t)$ based on (18) and input it into the actor network;
    The actor network outputs the corresponding action $\mathbf{a}(t)$ and adjusts it based on (21);
    Adding noise to the adjusted action by (25), and then execute it on the network;
    The agent calculates the local reward $R(t)$ according to (22) and the environment enter to the next state $\mathbf{s}(t+1)$;
    Stores the experience tuple $(\mathbf{s}(t), \mathbf{a}(t)(t), R(t), \mathbf{s}(t+1))$ into Memory $\mathcal{D}$;
    Soft update the target networks of central trainer according to (23);
    if No. stored tuples $\geq \frac{1}{3}|\mathcal{D}|$ **then**
      Sample a mini-batch with Ω transitions from $\mathcal{D}$;
      Update the critic network by minimizing the loss in (26);
      Update the actor network by maximizing the policy gradient in (29).
    end if
  end for
end for

follows

$$\boldsymbol{\theta}_Q \leftarrow \boldsymbol{\theta}_Q - \beta_Q \nabla_{\boldsymbol{\theta}_Q} L(\boldsymbol{\theta}_Q), \tag{28}$$

where β_Q is the learning rate of the critic network.

The optimization goal of the actor network is to obtain the maximum state-action function Q. Hence, considering the fact that the state-action function Q is differentiable and the action space is continuous, the actor network can be updated by the policy gradient with the ascent factor as follows

$$\nabla_{\boldsymbol{\theta}_\mu} J(\boldsymbol{\theta}_\mu) = \frac{1}{\Omega} \sum_{i=1}^{\Omega} \nabla_{\mathbf{a}} Q(\mathbf{s}, \mathbf{a}|\boldsymbol{\theta}_Q)|_{\mathbf{s}=\mathbf{s}(i), \mathbf{a}=\mu(\mathbf{s}(i))} \nabla_{\boldsymbol{\theta}_\mu} \mu(\mathbf{s}|\boldsymbol{\theta}_\mu)|_{\mathbf{s}(i)}. \tag{29}$$

Algorithm 2 gives the specific training process of the LSTM-DDPG based RIS control algorithm, which is embedded in the RIS controller.

Through sufficient exploration and training, DDPG will converge and learn the optimal policy $\mu^*(\mathbf{s}|\boldsymbol{\theta}_\mu^*)$ for controlling the RIS amplification power matrix and phase shift matrix. If there are no large fluctuations in the system parameters (e.g., M, K E_{max}^H), the network in DDPG no

longer needs to be retrained. In the online applications, based on the learned policy μ^*, the active RIS can design $\mathbf{P}$ and $\mathbf{\Theta}$ reasonably for the current system environment.

C. Complexity Analysis and Convergence Proof

1) Complexity Analysis of LSTM algorithm: The LSTM based algorithm contains a three-layer network structure, i.e., an input layer, LSTM layer, and an output LSTM layer. The activation function of both LSTM layer and output LSTM layer are 'tanh', and the optimization function of the whole network is 'RMSprop'. The number of neurons contained in the input layer, LSTM layers, and output layer are defined as L_i, L_1, and L_o, respectively. The input data size of the input layer is $L_i = 6$, where the first 5 are the user communication probabilities for 5 time slots and the last one characterizes the dimension of the input data. The output of the LSTM algorithm is the communication probability of a user at the current moment, and its dimension is $L_o = 1$. According to [40], the computational complexity of the LSTM layer is $\mathcal{O}(W1)$, where $W1 = 4L_1(L_i + b1 + L_1)$, and the complexity of the output LSTM layer is $\mathcal{O}(W2)$, where $\mathcal{O}(W2) = 4L_2(L_1 + b2 + L_o)$, $b1$ and $b2$ are the bias in the two LSTM layers. Then, the complexity of the proposed LSTM based prediction algorithm is $\mathcal{O}(W1 + W2)$.

2) Complexity Analysis of DDPG algorithm: In the proposed DDPG based RIS control algorithm, there are four DNNs, i.e., actor and critic main networks, and two target networks with the same structure as the main networks. Among them, the actor network contains input layer, output layer and three hidden layers with l_i neurons in the i-th layer. According to (18) and (19), the number of neurons in the input layer and output layer of the actor network is $l_0^a = k + 1$, $l_4^a = 2M$, respectively. The rectified linear activation function (ReLU) is used in both hidden layers, and the sigmoid activation function is used for the output layer. The actor network also contains an input layer, an output layer, and three hidden layers with l_i^c neurons in the i-th layer.

- Application complexity: During the online application, only the actor network needs to be executed, and for any input environment state $\mathbf{s}$, the trained actor network outputs corresponding action $\mathbf{a}$. According to the connection and calculation principle of the actor network, we can get a moderate computational complexity of the process from input to output that is as $\mathcal{O}(\sum_{i=0}^{3} l_i^a l_{i+1}^a)$.
- Training complexity: In the training process, both the actor network and critic network need to be trained, and the most intuitive complexity is caused by the back propagation.

Besides, the training process needs the prediction results from the target actor network and target critic network. Thus, a single back propagation training step for the proposed DDPG structure will contribute the complexity of $\mathcal{O}(\sum_{i=0}^{3} 2l_i^a l_{i+1}^a + \sum_{i=0}^{3} 2l_i^c l_{i+1}^c)$. In addition, it can be seen from Algorithm 2 that until the number of tuples stored in the replay memory $\mathcal{D}$ exceeds $\geq \frac{1}{3}|\mathcal{D}|$, the agent is only explored and not trained. Therefore, for the whole training process, the overall complexity of the DDPG based algorithm can be calculated as $\mathcal{O}\left((N^{all}T^{all} - \frac{1}{3}|\mathcal{D}|)\Omega(\sum_{i=0}^{3} 2l_i^a l_{i+1}^a + \sum_{i=0}^{3} 2l_i^c l_{i+1}^c) + \frac{1}{3}|\mathcal{D}|(\sum_{i=0}^{3} l_i^a l_{i+1}^a)\right)$.

In this paper, the number of neurons in the hidden layer of the actor network and the critic network are set to $l_1^a = l_1^c = 256$, $l_2^a = l_2^c = 256$, and $l_3^a = l_3^c = 128$. In this LSTM based algorithm, the numbers of neurons of two LSTM layers are set to $L_1 = 64$. Due to the simple structure of the LSTM network and the small numbers of neurons in each layer, the complexity of this LSTM algorithm is very low. The DDPG algorithm has higher complexity compared to LSTM, but its algorithm complexity is very low compared to the DRL algorithm with multiple agents. In addition, the state of the DDPG is a local observation with low dimensionality and does not require additional interaction with the users, which also greatly reduces the application complexity of the LSTM-DDPG algorithm. Based on the development and application of integrated development technology and software-defined networking technology, embedding LSTM and DDPG into the controller of RIS can be easily implemented with acceptable complexity.

3) Convergence Proof: Theorem 1: The proposed DDPG algorithm can converges.

Proof: Since the state space and the action space in the RIS-aided EH-NOMA wireless environment are finite, and all pairs $\{(\mathbf{s}(\mathbf{t}), \mathbf{a}(t)|t \in N^+)\}$ can be visited infinitely. In each training step t, the agent RIS can obtain an experience tuple $(\mathbf{s}(t), \mathbf{a}(t)(t), R(t), \mathbf{s}(t+1))$,then the Q function of critic network can be updated by:

$$\begin{aligned} Q(\mathbf{s}(t), \mathbf{a}(t)) =& Q(\mathbf{s}(t), \mathbf{a}(t)) + \alpha(\mathbf{s}(t), \mathbf{a}(t) \\ & [R(t) + \gamma \max_{\mathbf{a}} Q(\mathbf{s}(t+1), \mathbf{a}) - Q(\mathbf{s}(t), \mathbf{a}(t))], \end{aligned} \tag{30}$$

where $\alpha(\mathbf{s}, \mathbf{a}) = 0$ unless $(\mathbf{s}, \mathbf{a}) = (\mathbf{s}(t), \mathbf{a}(t))$. The Q function is intended to approximate the optimal Q function Q^* of the MDP. By subtracting $Q^*(\mathbf{s}(t), \mathbf{a}(t))$ from both the left and right sides of the above equation, the following equation can be obtained

$$\Psi(\mathbf{s}(t), \mathbf{a}(t)) = Q(\mathbf{s}(t), \mathbf{a}(t)) - Q^*(\mathbf{s}(t), \mathbf{a}(t)), \tag{31}$$

where

$$\begin{aligned}\Psi(\mathbf{s}(t),\mathbf{a}(t)) &= (1-\alpha)\Psi(\mathbf{s}(t),\mathbf{a}(t)) + \alpha(\mathbf{s}(t),\mathbf{a}(t))G(\mathbf{s}(t),\mathbf{a}(t)),\\ G(\mathbf{s}(t),\mathbf{a}(t)) &= [R(t) + \gamma \max_{\mathbf{a}} Q(\mathbf{s}(t+1),\mathbf{a}) - Q^*(\mathbf{s}(t),\mathbf{a}(t))].\end{aligned} \tag{32}$$

Because $\sum_{t=1}^{\infty}\alpha = \infty$ and $\sum_{t=1}^{\infty}\alpha^2 < \infty$, according to **[?]**, $\Psi(\mathbf{s}(t),\mathbf{a}(t))$ converges to zeros w.p.1 if:

1)$\|\mathbb{E}[G(\mathbf{s}(t),\mathbf{a}(t))|G]\|_\infty \le \gamma\|\Psi(\mathbf{s}(t),\mathbf{a}(t))\|_\infty$ with $\gamma < 1$.

2)var$[G(\mathbf{s}(t),\mathbf{a}(t))|G] \le C(1 + \|\Psi(\mathbf{s}(t),\mathbf{a}(t))\|_\infty^2)$, with a positive constant C.

First, the derivation of $\mathbb{E}[G(\mathbf{s}(t),\mathbf{a}(t))|G]\|_\infty$ is performed as follows

$$\begin{aligned}\mathbb{E}[G(\mathbf{s}(t),\mathbf{a}(t))|G]\|_\infty &= Pr(\mathbf{s}(t+1)|\mathbf{s}(t),\mathbf{a}(t))G(\mathbf{s}(t),\mathbf{a}(t))\\ &\le \gamma\|Q(\mathbf{s}(t),\mathbf{a}(t)) - Q^*(\mathbf{s}(t),\mathbf{a}(t))\|_\infty\\ &= \|\Psi(\mathbf{s}(t),\mathbf{a}(t))\|_\infty.\end{aligned} \tag{33}$$

Then, the var$[G(\mathbf{s}(t),\mathbf{a}(t))|G]$ can be calculated as

$$\text{var}[G(\mathbf{s}(t),\mathbf{a}(t))|G] = \text{var}[R(t) + \gamma \max_{\mathbf{a}} Q(\mathbf{s}(t+1),\mathbf{a})|G]. \tag{34}$$

Since $R(t) = r(\sum_{k=1}^{K}\mathbb{1}_{R_k(t)\geqq R_0})$ is bounded, then we can obtain

$$\text{var}[G(\mathbf{s}(t),\mathbf{a}(t))|G] \le C(1 + \|\Psi(\mathbf{s}(t),\mathbf{a}(t))\|_\infty^2). \tag{35}$$

Therefore, $\Psi(\mathbf{s}(t),\mathbf{a}(t))$ can converge to zero w.p.1, which means that the critic network of the proposed DDPG algorithm can converges to the optimal Q function $Q^*(\mathbf{s},\mathbf{a})$.

Then, for any state $\mathbf{s}$, the optimal action $\mathbf{a}^*$ can be selected based on the optimal function $Q^*(\mathbf{s},\mathbf{a})$, i.e.,

$$\mathbf{a}^*(t) = arg\max_{\mathbf{a}} Q^*(\mathbf{s}(t),\mathbf{a}). \tag{36}$$

The proof is completed. ■

V. Simulation Results and Discussions

In this section, we verify the performance of the proposed LSTM-DDPG algorithm in downlink active RIS-aided EH-NOMA networks. First, the accuracy of the LSTM based UCS prediction algorithm is verified, and then we examine the performance advantages of NOMA over OMA in active RIS EH networks. In addition, we compare the performance of active and passive RIS in the EH-NOMA network. Finally, the proposed LSTM-DDPG algorithm is compared with several other benchmark algorithms. Considering the actual communication scenario, the positions of both BS and RIS are fixed, and their 3D position coordinates are set to (0 m, 0 m, 0 m) and

TABLE I
SIMULATION PARAMETER SETTING

Parameter	Description	Value	Parameter	Description	Value
B	bandwidth	1 MHz	τ_μ, τ_Q	soft updating factor	0.01
r	reward parameters	10	p_k	transmitting power	0.1 W
E_{max}^H	maximum arrive energy	0.6 W	η	EH efficiency coefficient	0.9
$\|\mathcal{D}\|$	capacity of memory	10000	C_0	pass loss at reference distance	-30 dB
T^{all}	episode number	200	N^{all}	total step in each episode	200
Ω	size of mini-batch	40	β_μ, β_Q	learning rate	0.001
$\alpha_{B,k}$	pass loss exponent BS-users	3.5	$\alpha_{B,S}$, $\alpha_{S,k}$	pass loss exponent BS-RIS	2.2

(100 m, 100 m, 50 m), respectively. All users are on the right side of the BS and RIS, and they are randomly distributed in a semicircle with a radius of 200m to 500m from the BS. In all simulations, $\xi = 0.9$ is set to characterize the NOMA decoding error due to imperfect CSI. The parameters related to solar and RF energy harvesting in the energy model are set with reference to [36] and [37], respectively. The energy of the fully charged solar panel is 50 joules. Unless otherwise specified, the simulation parameters are given in Table I, which follows the simulation parameters setting in [27], [28].

A. Performance Verification of LSTM based Prediction Algorithm

First, we verify the performance of the proposed LSTM based prediction algorithm. The performance of the LSTM algorithm for a system containing four users is verified in Fig. 3. The real communication probabilities data of the four users are generated based on a random walk model, and the initial probability for each user is 0.6. Specifically, a series of 1000 time slots of real data were generated for each user, and the communication probability of each user in each time slot is a random value in $[0, 1]$. These 1000 data will be grouped in 5 time slots to produce 955 data sets, where the communication probability data for every 5th time slot is the input to the LSTM and the label is the communication probability for the 6th time slot. For the 955 datasets generated, 70% were used for training and the left 30% for testing. In Fig. 3, the

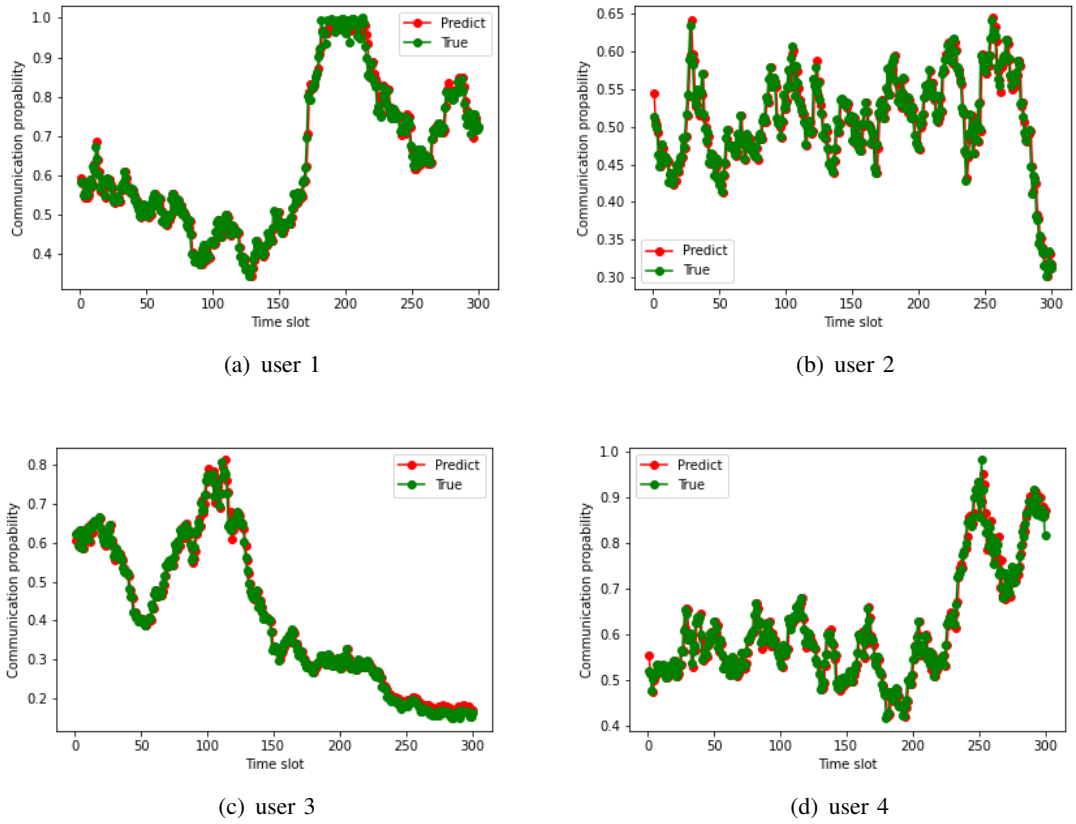

(a) user 1

(b) user 2

(c) user 3

(d) user 4

Fig. 3. Prediction effectiveness of LSTM based algorithm.

true data is the communication probability produced by the random model, and the predict data is the estimated output of the LSTM based algorithm.

As can be seen from Fig. 3, the LSTM-based prediction algorithm achieves a very high prediction accuracy. The predicted user communication probability and the real communication probability highly overlap, which proves the convergence of LSTM based prediction algorithm. The accuracy of the prediction can provide important guarantees for the subsequent design of the RIS amplification matrix and phase shift matrix. All subsequent simulation results are obtained based on the LSTM algorithm.

Fig. 4 further validates the performance of the LSTM based prediction algorithm. Specifically, we compare the performance of the proposed LSTM-DDPG algorithm with the DDPG based algorithm on perfect UCS information. In addition, to further verify the performance of the proposed LSTM, the gated recurrent unit (GRU) algorithm is introduced in the simulation for comparison, and the performance of GRU-DDPG based algorithm is verified. The comparison of

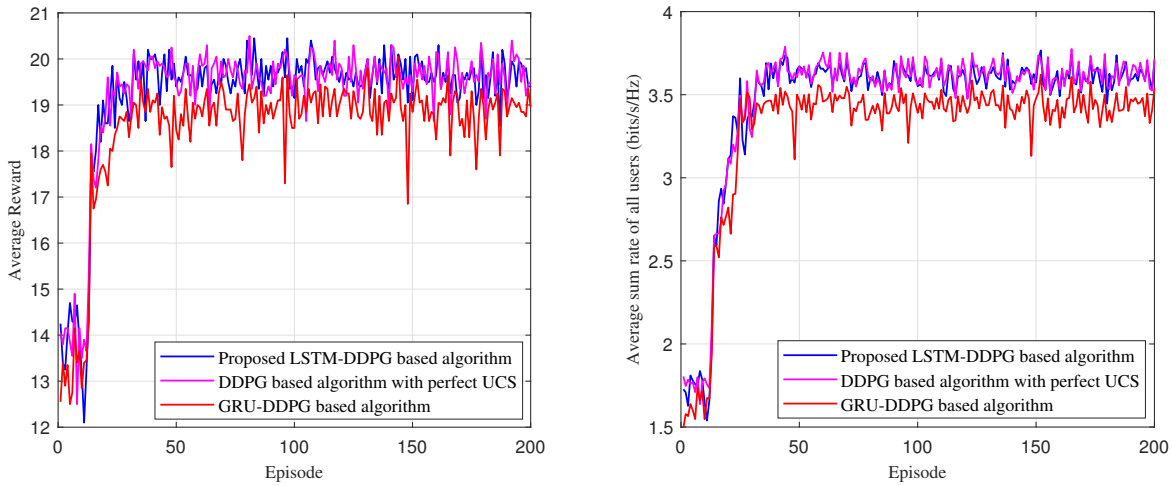

Fig. 4. Performance comparison with and without LSTM, where $R_0 = 0.6$ bits/s/Hz, $K = 4$, $L = 25$, $p_k = 0.01W$, and $M = 100$.

the average reward and the average communication success ratio of the system is given in Fig. 4. It can be seen that the performance obtained by the proposed LSTM-DDPG algorithm and the DDPG based algorithm with perfect UCS is almost similar. In the DDPG algorithm, the perfect UCS information does not have a significant advantage over the LSTM based prediction of the UCS information, which fully demonstrates the effectiveness of the designed LSTM algorithm. In addition, it can be seen from Fig. 5 that the performance of the GRU-DDPG-based algorithm is about 4% lower than that of the proposed algorithm, and the stability of this algorithm is not good enough.

B. Verification of NOMA Performance Advantages

To verify the advantages of using NOMA in the EH active RIS-aided network, we compared the performance of NOMA and OMA in this network in Fig 5. Two classical DRL algorithms: DDPG and AC are used to perform the design of the amplification power matrix and phase shift matrix of the active RIS. Note that all DRL based algorithms in the simulation use the same DRL framework, i.e., they use the same action, state, and reward functions designed in Section IV-A. The training and application results are obtained based on the deep learning framework in TensorFlow 1.14.0.

First, it can be seen that with training, the performance of both DDPG and AC algorithms can gradually improve and achieve convergence after about 25 episodes in both NOMA and OMA

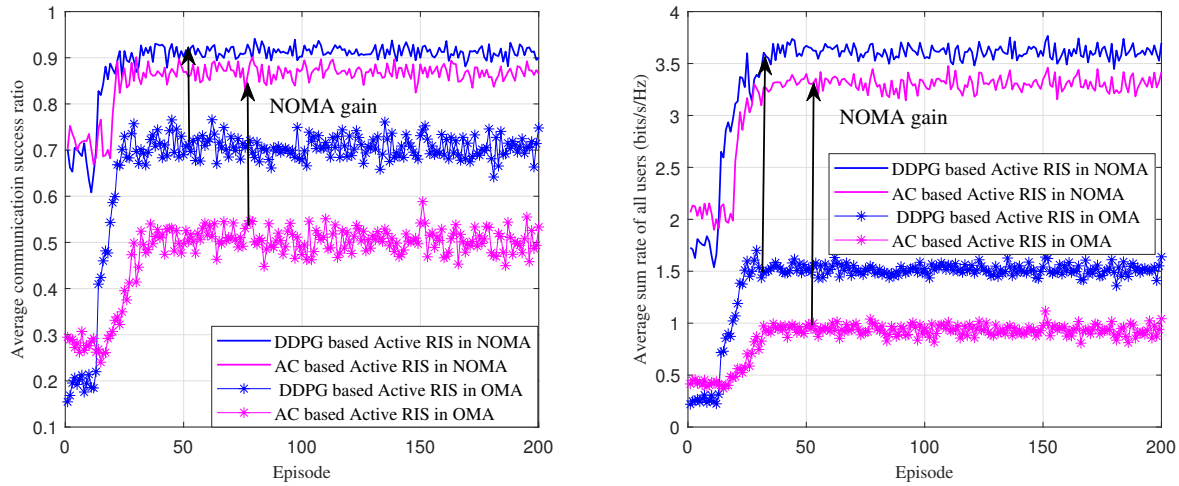

Fig. 5. Performance comparison of in active RIS, where $R_0 = 0.6$ bits/s/Hz, $K = 4$, $L = 25$, and $M = 100$.

modes, which validates the effectiveness of the proposed DRL framework. More importantly, it is evident that both algorithms are able to obtain better performance in NOMA mode with respect to OMA. The arrows in the diagram visualize the advantages of NOMA technology compared to OMA. Specifically, in the proposed DDPG based algorithm, the average communication success ratio is improved by 29.28% and the average sum rate is improved by 137% in NOMA mode with respect to OMA. The communication success ratio and sum rate gains obtained by NOMA in the AC algorithm can also reach about 72.66% and 254%, respectively. Simulation results show that NOMA can obtain much better performance in active RIS networks compared to OMA, which indicates that NOMA has better adaptability to active RIS networks.

Fig. 6 shows the effect of channel estimation error on the performance of the proposed LSTM-DDPG algorithm. $\xi = 100\%$ indicates that the channel estimation error is 0. The smaller the value of ξ characterizes the larger the SIC error of NOMA. It can be seen that the larger the SIC error, the worse the performance obtained by the system, and when $\xi < 90\%$, the average communication success rate of the system is below 0.9.

C. Performance Comparison of Active RIS and Passive RIS in the EH-NOMA Networks

Fig. 7 shows the performance of the two DRL algorithms, DDPG and AC, under active and passive RIS, respectively. Note that since the system performance is very poor (below the average communication success rate of 0.1) in the passive RIS system when the user transmit power is not high ($p_k = 0.01W$), the transmit power of the user is set to $p_k = 0.05W$ in all

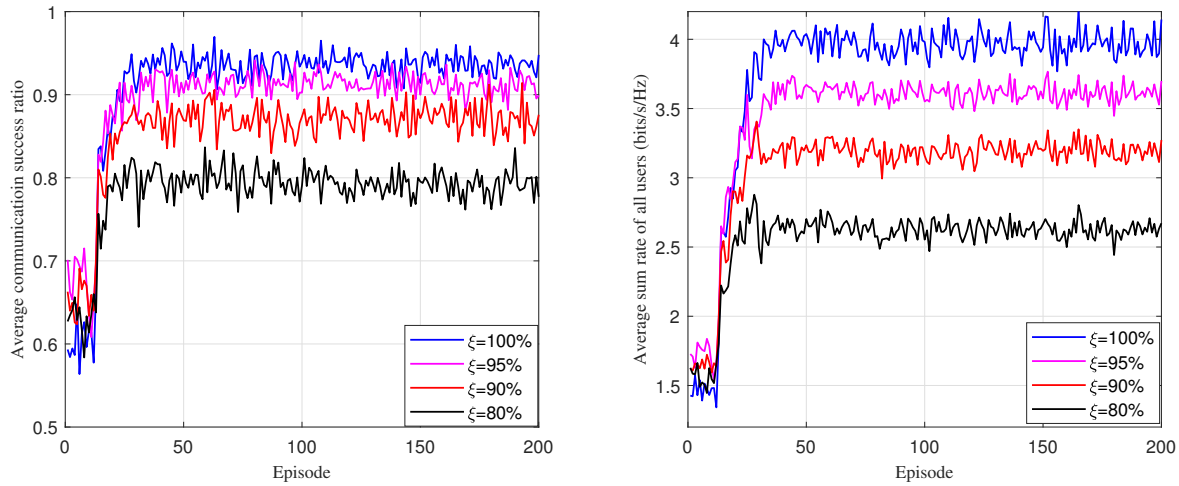

Fig. 6. Impact of the NOMA decoding error ξ on system performance, where $R_0 = 0.6$ bits/s/Hz, $K = 4$, $L = 25$, and $M = 100$.

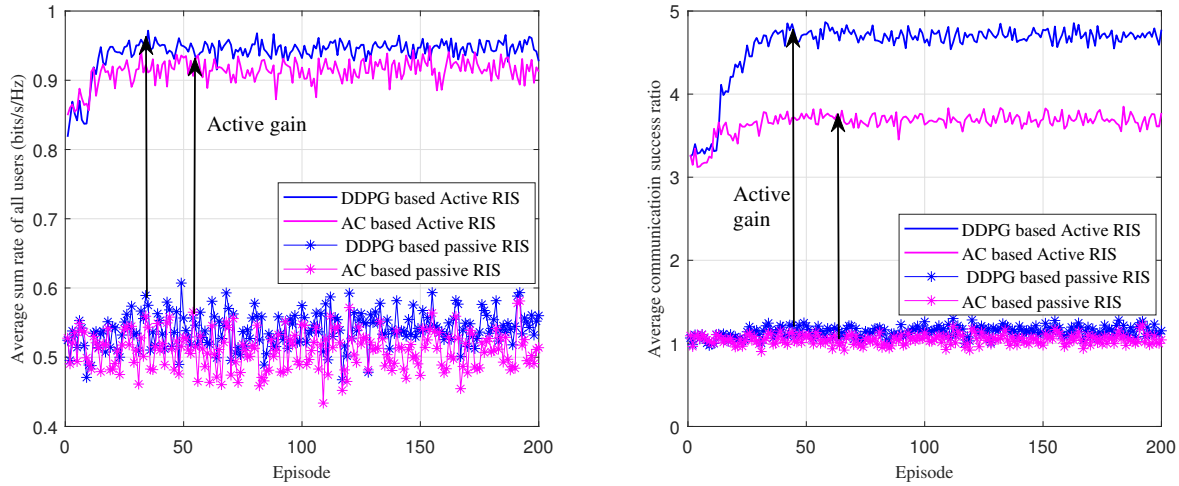

Fig. 7. Performance comparison of active and passive RIS with NOMA, where $R_0 = 0.6$ bits/s/Hz, $K = 4$, $L = 25$, and $M = 100$.

subsequent simulations for better performance comparison. All the users in the simulation are accessing the network by NOMA. As shown in Fig. 7, the control of the phase matrix by the two DRL algorithms do not achieve any performance improvement under passive RIS, so both algorithms obtain similar performance. However, under active RIS, both DRL algorithms can achieve a significant performance improvement after a short training period. This is because the amplification matrix and the phase shifting matrix are jointly controlled in the active RIS.

The advantages of active RIS over passive RIS can be clearly seen in Fig. 7. Specifically, in

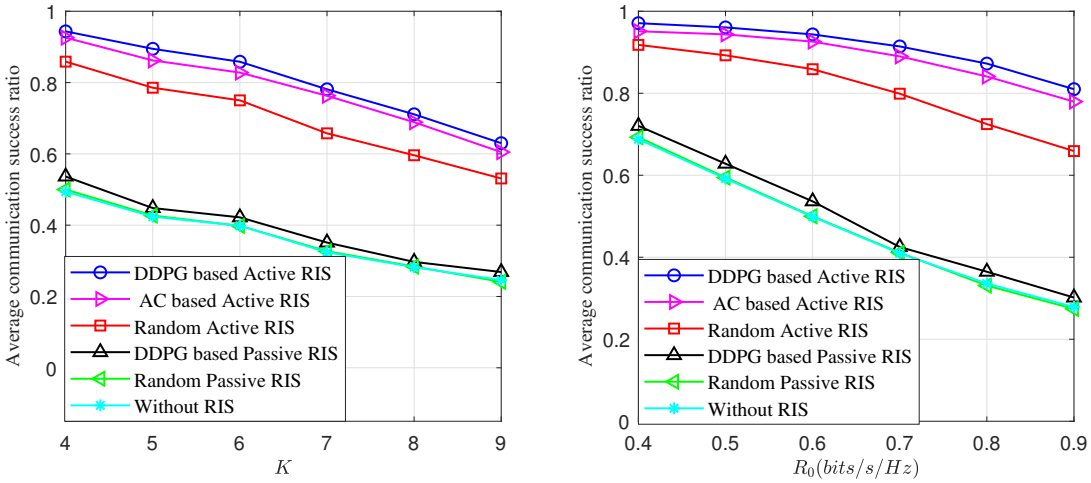

Fig. 8. Application performance comparison of different algorithms, where $L = 25$ and $M = 100$.

the proposed DDPG algorithm, the communication success ratio and the sum rate performance of the active RIS are improved by 73.72% and 306.3%, respectively, compared to the passive RIS. The active RIS in the AC algorithm also obtains 79.3% and 251% performance gains in these two performances, respectively. Last but not least, both Figs. 5 and 7 show that the DDPG algorithm achieves better training results than the AC algorithm. This is because the DDPG algorithm introduces the structure of DQN to improve the stability and convergence of AC.

D. Application Performance Testing of the Proposed LSTM-DDPG Algorithm

Finally, the application performance of the proposed LSTM-DDPG algorithm is tested. Considering that the optimization objective of our work is to maximize the communication success ratio of the whole system, we test the ratio of the trained algorithm. The data for training and testing are generated simultaneously and distributed in a $7:3$ ratio. To better demonstrate the superiority of the proposed algorithm, several benchmark algorithms are introduced for comparison via different system parameters in Figs. 8 - 9. It can be seen that the performance of the passive RIS network and the without RIS network is similarly poor under various network parameters, and the networks without RIS have the worst performance. This is because there is no power amplification in these networks, thus failing to meet the required rate threshold and causing the communication to fail.

In Fig. 8 (a), we examined the impact of the number of users K on the system performance

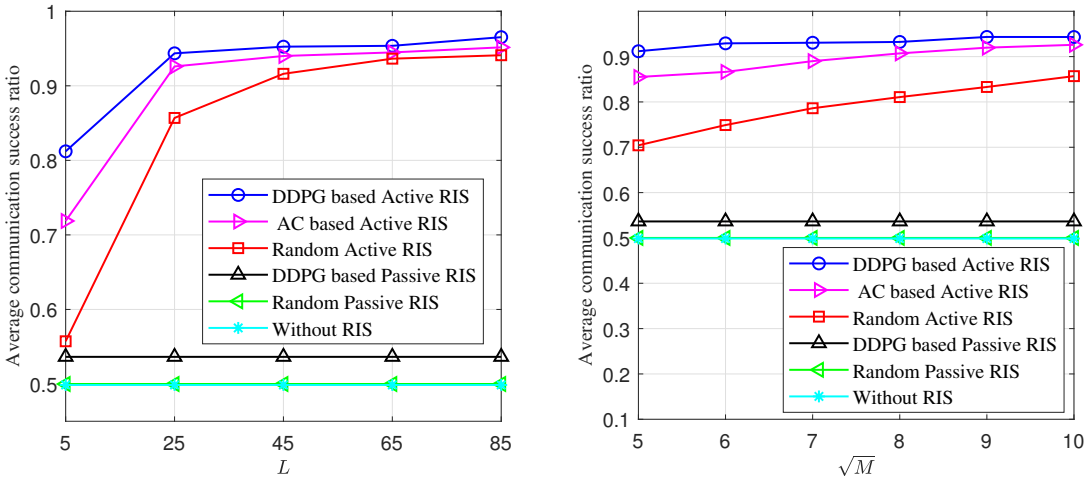

Fig. 9. Application performance comparison of different algorithms, where $R_0 = 0.6 bits/s/Hz$ and $K = 4$.

of different algorithms with $R_0 = 0.6$ bits/s/Hz. It can be seen that the performance of all the algorithms gets worse as K increases. This is due to the fact that more co-channel interference will be caused by more users, which makes lower rates, and thus more users are unable to communicate successfully. It can be seen that the two DRL algorithms can obtain better performance compared to other algorithms, with the DDPG based algorithm obtaining the best communication success ratio. Although both algorithm apply active RIS, the random active RIS algorithm performs worse than the DRL based algorithm. This is because the amplification matrix and phase shift matrix in the random active RIS algorithm are not determined based on the current system state, but are determined randomly. In addition, it can be found that the proposed DDPG based algorithm can obtain better performance than other algorithms. Even when $K = 9$, the DDPG based algorithm still achieves the performance of about 0.63, outperforming the AC, random active RIS, DDPG based passive RIS, and random passive RIS algorithms about by 5%, 18.9%, 135.1%, and 156.1%, respectively.

Fig. 8(b) illustrates the impact of the rate threshold on all comparison algorithms with $K = 4$. As shown in Fig. 8(b), the performance of all algorithms deteriorates as R_0 increases. This is because a higher rate threshold means it is more challenging to achieve successful communication, which leads to more task failures. Also, it can be seen that even at $R_0 = 0.9$, the DDPG algorithm still obtains a communication success ratio of 0.81, which is 3.8%, 22.7%, and 170%

better than the AC, the random active RIS, and the DDPG based passive RIS, respectively.

Fig. 9 examines the effect of the maximum power amplification L and the number of RIS elements M on the performance of different algorithms, where $M = 100$ in Fig. 9(a), $L = 25$ in Fig. 9(b). It can be seen that the performance of the two passive RIS algorithms as well as the without RIS network is not affected by the parameters L and M. This is because in all three algorithms, the RIS does not amplify the received signal, and the increase in the number of RIS elements does not improve the user's communication success when the rate threshold R_0 is not very small (R_0 = 0.6 bits/s/Hz). In addition, it can be observed that the communication success ratio of the three active RIS algorithms improves significantly with increasing L and M, especially for the two DRL based algorithms, which further supports the validity of the Markov model of the designed DRL.Among all the algorithms, the proposed DDPG algorithm is able to achieve the best performance. Specifically, the proposed algorithm achieves a communication success ratio of 0.943 with $L = 100$ and $M = 100$, outperforming the AC, the random active RIS, DDPG based passive RIS, and random passive algorithm by 1.86%, 10.07%, 75.6%, and 88.6%, respectively.

VI. Conclusions

In this paper, we studied the RIS control for active RIS-aided EH-NOMA networks, where the RIS is powered by EH, and the UCS are dynamic. With the objective of maximizing the communication success ratio, an LSMT based algorithm was designed to predict the UCS. Based on the prediction results, a DDPG based algorithm was proposed for the joint control of the amplification matrix and phase shift matrix of the active RIS. The complexity of the LSTM based prediction algorithm and the DDPG based RIS control algorithm are analyzed. Sufficient simulation results demonstrated the effectiveness and superiority of the proposed algorithm in terms of the communication success ratio. Simulation results demonstrate the achievable performance improvement for our proposed scheme with respect to schemes of OMA, NOMA with passive RIS, and NOMA without RIS. In the future, we will consider the power allocation at the BS and further explore RIS control algorithms for more complex communication scenarios, such as systems containing multiple channels and (or) multiple antennas configured at the BS or users.

References

[1] Q. Wu and R. Zhang, "Intelligent reflecting surface enhanced wireless network via joint active and passive beamforming," *IEEE Trans. Wireless Commun.*, vol. 18, no. 11, pp. 5394–5409, Nov. 2019.

[2] Q. Wu and R. Zhang, "Towards smart and reconfigurable environment: Intelligent reflecting surface aided wireless networks," *IEEE Commun. Mag*., vol. 58, no. 1, pp. 106–112, Jan. 2019.

[3] X. Mu, Y. Liu, L. Guo, J. Lin, and N. Al-Dhahir, "Exploiting intelligent reflecting surfaces in NOMA networks: Joint beamforming optimization," *IEEE Trans. Wireless Commun.*, vol. 19, no. 10, pp. 6884–6898, Oct. 2020.

[4] C. Huang, A. Zappone, G. C. Alexandropoulos, M. Debbah, and C. Yuen, "Reconfigurable intelligent surfaces for energy efficiency in wireless communication," *IEEE Trans. Wireless Commun.*, vol. 18, no. 8, pp. 4157–4170, Aug. 2019.

[5] C. Huang, R. Mo, and C. Yuen, "Reconfigurable intelligent surface assisted multiuser MISO systems exploiting deep reinforcement learning," *IEEE J. Sel. Areas Commun.*, vol. 38, no. 8, pp. 1839–1850, Aug. 2020.

[6] Z. Zhang et al., "Active RIS vs. passive RIS: Which will prevail in 6G? " 2021, *arXiv:2103.15154*. [Online]. Available: http://arxiv.org /abs/2103.15154.

[7] P. Wang, J. Fang, X. Yuan, Z. Chen, and H. Li, "Intelligent reflecting surface-assisted millimeter wave communications: Joint active and passive precoding design," *IEEE Trans. Veh. Technol.*, vol. 69, no. 12, pp. 14960–14973, Dec. 2020.

[8] T. Hou, Y. Liu, Z. Song, X. Sun, and Y. Chen, "MIMO-NOMA networks relying on reconfigurable intelligent surface: A signal cancellation based design," *IEEE Trans. Commun.*, vol. 68, no. 11, pp. 6932–6944, Nov. 2020.

[9] Z. Zhang and L. Dai, "A joint precoding framework for wideband reconfigurable intelligent surface-aided cell-free network," *IEEE Trans. Signal Process.*, vol. 69, pp. 4085–4101, Aug. 2021.

[10] M. Najafi, V. Jamali, R. Schober, and H. V. Poor, "Physics-based modeling and scalable optimization of large intelligent reflecting surfaces," *IEEE Trans. Commun.*, vol. 69, no. 4, pp. 2673–2691, Apr. 2021.

[11] K. Liu, Z. Zhang, L. Dai, S. Xu, and F. Yang, "Active reconfigurable intelligent surface: Fully-connected or sub-connected?" *IEEE Commun. Lett.*, vol. 26, no. 1, pp. 167–171, Jan. 2022.

[12] E. Basar and H. V. Poor, "Present and future of reconfigurable intelligent surface-empowered communications," 2021, *IEEE Signal Process. Mag.* vol. 38, no. 6, pp. 146–152, Nov. 2021.

[13] C. You and R. Zhang, "Wireless communication aided by intelligent reflecting surface: Active or passive?" 2021, *IEEE Trans. Wireless Commun.* vol. 10, no. 12, pp. 2659–2663, Dec. 2021.

[14] K. Zhi, C. Pan, H. Ren, K. K. Chai, and M. Elkashlan, "Active RIS versus passive RIS: Which is superior with the same power budget?" *IEEE Commun. Lett.*, vol. 26, no. 5, pp. 1150–1154, May 2022.

[15] T. D. Ponnimbaduge Perera, D. N. K. Jayakody, S. K. Sharma, S. Chatzinotas, and J. Li, "Simultaneous wireless information and power transfer (SWIPT): Recent advances and future challenges," *IEEE Commun. Surveys Tuts.*, vol. 20, no. 1, pp. 264–302, 1th Quart. 2018.

[16] Z. Ding, X. Lei, G. K. Karagiannidis, R. Schober, J. Yuan, and V. Bhargava, "A survey on non-orthogonal multiple access for 5G networks: Research challenges and future trends," *IEEE J. Sel. Areas Commun.*, vol. 35, no. 10, pp. 2181–2195, Oct. 2017.

[17] M. Elhattab, M. A. Arfaoui, C. Assi, and A. Ghrayeb, "RIS-Assisted joint transmission in a two-cell downlink NOMA cellular system," *IEEE J. Sel. Areas Commun.*, vol. 40, no. 4, pp. 1270–1286, Apr. 2022.

[18] Z. Wang, T. Lv, J. Zeng and W. Ni, "Placement and Resource Allocation of Wireless-Powered Multiantenna UAV for Energy-Efficient Multiuser NOMA," *IEEE Trans. Wireless Commun.*, vol. 21, no. 10, pp. 8757–8771, Oct. 2022.

[19] F. Alanazi, "NOMA with energy harvesting using reconfigurable intelligent surfaces for Nakagami channels," *Signal, Image and Video Process.*, vol. 15, no. 8, 1837-1844, May 2021.

[20] F. Alanazi, "Non orthogonal multiple access with energy harvesting using reconfigurable intelligent surfaces for Rayleigh channels," *Wireless Pers. Commun.*, vol. 122, no. 3, 2161–2181, Feb. 2021.

[21] M. Diamanti, E. E. Tsiropoulou, and S. Papavassiliou, "The joint power of NOMA and reconfigurable intelligent surfaces in SWIPT networks," in *Proc. IEEE 22nd Int. Workshop Signal Process. Adv. Wireless Commun. (SPAWC)*, Sep. 2021, pp. 621–625.

[22] G. Zhang et al., "Hybrid Time-Switching and Power-Splitting EH Relaying for RIS-NOMA Downlink," *IEEE Trans. Cogn. Commun. Netw.*, vol. 9, no. 1, pp. 146-158, Feb. 2023.

[23] Z. Ding, R. Schober, and H. Vincent Poor, "No-pain No-gain: DRL assisted optimization in energy-constrained CR-NOMA networks," *IEEE Trans. on Commun.*, vol. 69, no. 9, pp. 5917-5932, Sep. 2021.

[24] Z. Shi, X. Xie, H. Lu, H. Yang, J. Cai and Z. Ding, "Deep Reinforcement Learning-Based Multidimensional Resource Management for Energy Harvesting Cognitive NOMA Communications," *IEEE Trans. Commun.*, vol. 70, no. 5, pp. 3110–3125, May 2022.

[25] N. C. Luong, *et al.*, "Applications of deep reinforcement learning in communications and networking: A survey," *IEEE Commun. Surveys Tuts.*, vol. 21, no. 4, pp. 3133–3174, 4th Quart., 2019.

[26] A. Faisal, I. Al-Nahhal, O. A. Dobre, and T. M. N. Ngatched, "Deep reinforcement learning for RIS-assisted FD systems: Single or distributed RIS?" *IEEE Commun. Lett.*, vol. 26, no. 7, pp. 1563–1567, Jul. 2022.

[27] X. Liu, Y. Liu, Y. Chen, et al."RIS enhanced massive Non-Orthogonal Multiple Access Networks: Deployment and passive beamforming design," *IEEE Syst. J.*,vol. 39, no. 4, pp. 1057–1071, Apr. 2021.

[28] R. Zhong, Y. Liu, X. Mu, Y. Chen, and L. Song, "AI empowered RIS-assisted NOMA networks: Deep learning or reinforcement learning? ," *IEEE J. Sel. Areas Commun.*, vol. 40, no. 1, pp. 182–196, Jan. 2021.

[29] J. Zhao, L. Yu, K. Cai, Y. Zhu, and Z. Han, "RIS-aided ground-aerial NOMA communications: A distributionally robust DRL approach," *IEEE J. Sel. Areas Commun.*, vol. 40, no. 4, pp. 1287–1301, Apr. 2022.

[30] A. Faisal, I. Al-Nahhal, O. A. Dobre, and T. M. N. Ngatched, "Deep reinforcement learning for optimizing RIS-assisted HD-FD wireless systems," *IEEE J. Sel. Areas Commun.*, vol. 25, no. 12, pp. 3893–3897, Dec. 2021.

[31] S. Wang, T. Lv, W. Ni, N. C. Beaulieu and Y. J. Guo, "Joint Resource Management for MC-NOMA: A Deep Reinforcement Learning Approach," *IEEE Trans. Wireless Commun.*, vol. 20, no. 9, pp. 5672-5688, Sept. 2021.

[32] E. Björnson and L. Sanguinetti, "Rayleigh fading modeling and channel hardening for reconfigurable intelligent surfaces," *IEEE Wireless Commun. Lett.*, vol. 10, no. 4, pp. 830–834, 2020.

[33] B. Xia, J. Wang, K. Xiao, Y. Gao, Y. Yao, and S. Ma, "Outage performance analysis for the advanced SIC receiver in wireless NOMA systems," *IEEE Trans. Veh. Technol.*, vol. 67, no. 7, pp. 6711–6715, Jul. 2018.

[34] M. Zeng, W. Hao, O. A. Dobre, Z. Ding, and H. V. Poor, "Power minimization for multi-cell uplink NOMA with imperfect SIC," *IEEE Wireless Commun. Lett.*, vol. 9, no. 12, pp. 2030–2034, 2020.

[35] Z. Shi, X. Xie, H. Lu, H. Yang, and J. Cai, "Deep reinforcement learning based dynamic user access and decode order selection for uplink NOMA system with imperfect SIC," *IEEE Wireless Commun. Lett.*, vol. 10, no. 4, pp. 710–714, 2020.

[36] C. Wang, J. Li, Y. Yang, and F. Ye, "A hybrid framework combining solar energy harvesting and wireless charging for wireless sensor networks," *IEEE INFOCOM 2016-The 35th Annual IEEE International Conference on Computer Communications*, 2016: IEEE, pp. 1–9.

[37] E. Boshkovska, D. W. K. Ng, N. Zlatanov, and R. Schober, "Practical Non-Linear Energy Harvesting Model and Resource Allocation for SWIPT Systems," *IEEE Commun. Lett.*, vol. 19, no. 12, pp. 2082–2085, Dec. 2015.

[38] Z. Yang, Y. Liu, Y. Chen, and N. Al-Dhahir, "Cache-aided NOMA mobile edge computing: A reinforcement learning approach," *IEEE Trans. Wireless Commun.*, vol. 19, no. 10, pp. 6899–6915, Oct. 2020.

[39] L. Wei, C. Huang, G. C. Alexandropoulos, C. Yuen, Z. Zhang and M. Debbah "Channel estimation for RIS-empowered multi-user MISO wireless communications," *IEEE Trans. Commun.*, vol. 69, no. 6, pp. 4144–4157, Jun. 2021.

[40] S. Hochreiter and J. Schmidhuber, "Long short-term memory," *Neural Comput.*, vol. 9, no. 8, pp. 1735–1780, Nov. 1997.

[41] V. Mnih, *et al.*, "Human-level control through deep reinforcement learning," *Nature*, vol. 518, no. 7540, pp. 529–533, 2015.